Industrial Engineering Journal
ISSN: 0970-2555
Volume : 51, Issue 04, April : 2022

Enhancement of CO_2RR product formation on Cu-ZnO-based electrodes by varying ink formulation and post-treatment methods

1.Sipuna Biswal 2. Monalisa Panda
Nalanda Institute Of Technology, Bhubaneswar
Department Of Basic Science & Humanities
Email id- SipunaBiswal@thenalanda.onmicrosoft.com, MonalishaPanda@thenalanda.onmicrosoft.com

Abstract

For the electrochemical CO2 reduction process, many catalysts have been described with better performance, such as extended lifespan and increased selectivity (CO2RR). Yet, very little is known about how the structure and pre-treatment of the electrodes affect this catalytic layer response. As a result, we describe in this article how changing the ink composition and applying an electrode treatment thereafter to the catalytic environment of a Cu-ZnO-carbon black catalyst before performing CO2RR. We also discuss the effects on the performance of the CO2RR of various solvents, ionomers, and additives used to prepare the ink as well as post-treatment activities like as pressing and sintering the produced electrodes. Although all electrodes having the same catalyst, there are notable variances in hydrophobicity, surface morphology,

1.Introduction

Tackling the negative effects of climate change requires new disruptive technologies. Along this line, the conversion of the greenhouse gas CO_2 into valuable chemicals is suggested to be key to achieve this goal [1]. A potential method to convert this molecule to e.g. multicarbon products is the use of surplus electricity from renewable energy sources to electrochemically drive this reduction. While the catalyst is key to facilitate the catalytic conversion of CO_2, the electrode assembly and reactor setup play an equally important role to achieve efficient CO_2 reduction reaction (CO_2RR) processes of industrial relevance. Along this line, a minimum current density of 200 mA cm^{-2} with Faraday efficiencies (FEs) of at least 60% for multicarbon products are required [2–5]. Herein, utilization of gas diffusion electrodes (GDEs) in continuously driven flow cells showed promising results toward this aim. High achievable current densities and cell voltages below 3 V further support the promising role of GDEs for industrial CO_2RR toward multicarbon products—e.g. Li *et al* reached a FE for ethanol of 41% at a partial current density of 250 mA cm^{-2} using an $Ag_{0.14}/Cu_{0.86}$ catalyst [6–10].
Among the large variety of reported catalysts, especially combinations of copper and zinc were shown to support the formation of C–C coupling products such as ethylene, ethanol, acetic acid, or propanol [11–13]

The C–C coupling was reported to follow a tandem mechanism with the Zn sites facilitating the CO_2 reduction to CO and the Cu sites allowing for subsequent CO coupling [14]. As of now, Cu seems to be essential for C–C bond formation and is currently the only metal electrocatalyst reported to enable this coupling step. However, many studies are limited to low current densities and with it low conversion rates. With respect to large-scale applications and the therein needed parameters, GDEs offer unique possibilitiesto adjust the three-phase boundary (TPB) at the catalyst by optimizing the interaction of CO_2, catalyst, andwater/protons and allow for efficient CO_2 reduction at current densities >200 mA cm^{-2}. This behavior is enabled by the efficient gas transport to the active sites of the catalyst, while simultaneously suppressing theparasitic hydrogen evolution reaction (HER). For example, Cu-ZnO-based GDEs allowed for FEs of up to 78% for C_{2+} products (mainly ethylene and ethanol) at potentials of 0.73 V and current densities of 466 mA cm^{-2} [11]. Comparable high FEs of 60% C_2H_4 and 25% EtOH [15] were reported for Cu-Ag basedGDEs at −0.7 V with current densities of 180 mA cm^{-2}. Additionally, B-Cu-Zn-based GDEs were reported to form C_{2+} products with FEs of up to 79% [16].

In addition to the catalysts, the choice of process parameters during electrolysis was also shown to have a major influence on the product distribution and thus overall electrode performance. Especially the influence of the used electrolyte [17–19] alongside pH changes on the local environment, as well as the effects of temperature [20, 21] or pressure [22, 23] on the electrocatalytic performance and product distribution were reported as key factors. Beyond these process parameters and the choice of appropriate catalysts, Berlinguette, Schuhmann, as well as Apfel and coworkers recently showed the impact of electrode fabricationand composition itself on the overall product distribution by preparing various catalyst inks with different solvents in Cu- and Ag-GDEs [16, 24, 25].

The use of different solvents, carbon materials or even ionomer additives in the catalyst-containing ink accounted for significant differences in the observed FE in CO_2 reduction to the various products formed. Especially, altered catalytic behavior utilizing different solvents occurred due to different agglomeration behavior of the ionomer that led to different microstructures of the catalyst layer. This change in return influences the CO_2RR product formation. Interestingly, similar observations were also made for fuel cell inks in the context of polymer electrolyte membrane fuel cells [26]. Additionally, the usage of ionomers like Nafion was reported to improve the electrolysis by contributing to a faster re-supply of CO_2 and therefore increase the TPB formation where the CO_2RR takes place [27].

Furthermore, Chen and Su *et al* modulated the hydrophobicity within the catalyst layer of Cu-particle containing GDEs for the CO reduction using different amounts of polytetrafluoroethylene (PTFE).
Increasing the binder content up to 25 wt.% increased the contact angle from 132.8° (5 wt.%) to 147.2° and led to higher C_{2+} product formation compared to 5 or 13 wt.%, probably due to enhanced CO supply at the catalyst [28]. Besides an increased supply of reactant gases, the increased hydrophobicity prevents the GDEs from flooding and stabilizes the electrodes during operation [27].
Additionally, the fabrication method influences the GDE's composition and therefore also the product distribution [29]. Along this line, Lees *et al* showed that airbrushed, drop-casted and ultrasonic spray coated electrodes revealed differences in their Nafion content distributions inside the catalyst layer accompanied by an overall altered CO_2RR performance. These studies clearly show that research in electrocatalysis must not be exclusively focused on the catalyst systems but also on the application and modification of catalyst layers.

We herein further demonstrate the importance of the ink formulation and show that likewise

post-treatment steps—like pressing and sintering of the sprayed electrode—have a significant effect on the GDEs' performance in CO_2RR processes. We believe that this opens a completely new space of parameters that must be understood with regard to the resulting physico-chemical properties and effects on GDEs foroptimized CO_2RR.

2.Results and discussion

Experimental design strategy and electrode preparation

A carbon black (CB) supported copper–zinc catalyst was synthesized via an impregnation process (experimental part). The total anticipated metal loading on the CB support was 10 wt.% and the Cu:Zn mass ratio was adjusted to 85:15. Since promising results had already been obtained with impregnated CuCB catalysts [25], their impregnation process was adapted and extended to the additional use of Zn. This process includes partial surface oxidation of the CB, subsequent treatment with suitable metal salts and final reduction under H_2 atmosphere. In the current study, Zn was additionally added to facilitate the formation of C_{2+} products, especially alcohols. Notably, while the Cu:Zn ratio of 85:15 refers to the pure metal content, data from powder x-ray diffraction (figure S1) points toward the presence of a ZnO bulk material under the herein used conditions. In addition, inductively coupled plasma optical emission spectroscopy (ICP-OES) measurements reveal a slightly altered Cu:Zn ratio of 78.5:14.0 and a lower metal loading of 9.25 wt.% (instead of 10 wt.%) in the final electrode.

Industrial Engineering Journal
ISSN: 0970-2555
Volume : 51, Issue 04, April : 2022

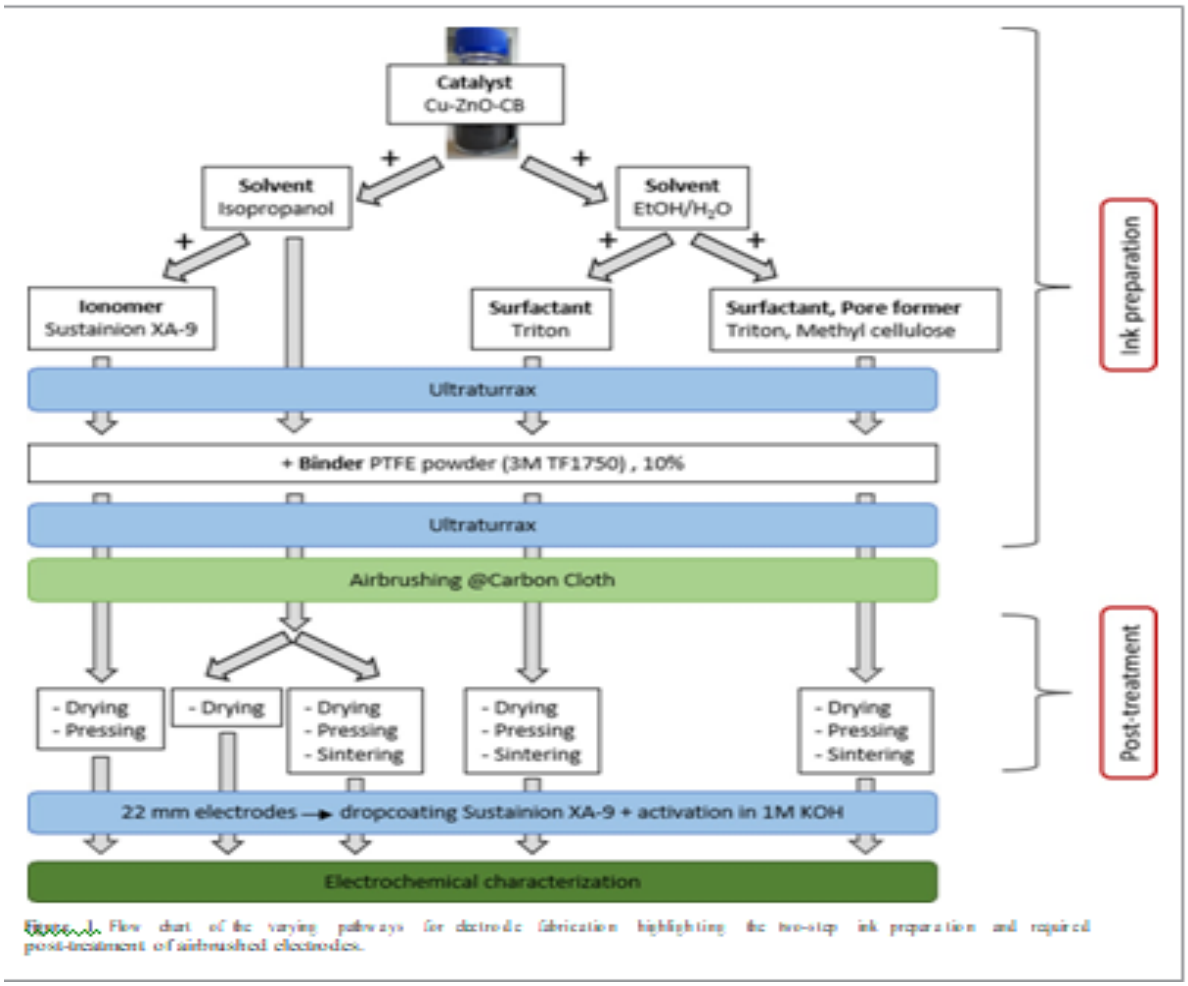

Figure 1. Flow chart of the varying pathways for electrode fabrication highlighting the two-step ink preparation and required post-treatment of airbrushed electrodes.

Industrial Engineering Journal
ISSN: 0970-2555
Volume : 51, Issue 04, April : 2022

Figure 1 provides a general overview of the different ink compositions and post-treatment steps. A more detailed overview including a designation of the electrodes (IPA1–IPA5, Water1 and Water2) is given in table 1.

For all GDEs utilized in this study, the catalyst ink was deposited on a gas diffusion layer (GDL) by airbrushing. In addition to different ink compositions, the preparation method also includes subsequent pressing of the electrode to improve adhesion between the GDL and the catalyst layer as well as sintering to remove organic components by thermal decomposition. Pressing was conducted either at room temperature(RT) or at 130 ˚C. After pressing, the electrodes were partially sintered at 340 ˚C for 15 min in a muffle furnace under atmospheric conditions. Noteworthily, sintering also softens the PTFE and is thus supposed toincrease its binding capabilities.

Notably, the same batches of catalyst and PTFE powder (3 M TF1750) were used for the catalyst layer preparation for all presented electrodes throughout this study. PTFE was selected as a binder material due to its hydrophobicity, known to increase the gas transport within the catalyst layer by minimizing pore flooding. Within this study, inks can be divided into two subgroups based on the solvent used to prepare the dispersions: those with (a) ethanol/water and (b) isopropanol. For the isopropanol-based inks (left strand in figure 1), we also investigated on how the usage of an additional anion exchange additive, the XA-9 ionomer, will alter the CO_2RR activity of the GDE. Similarly, ink compositions based on ethanol/water mixtures were investigated (right strand in figure 1). Along this line, it is worth mentioning that Mowbray *et al* reported a higher FE_{CO} during CO_2RR for Ag-based GDEs when electrodes were sprayed with ethanol instead of propanol-based inks [24].

In addition to the catalyst, ethanol and water, Triton X-100 and 1 wt.% aqueous methyl cellulose solution were used as additional ink components. Triton X-100 as a non-ionic surfactant is expected to contribute to the formation of a stable ink dispersion during the air-brushing step and has been used before to modulate

Industrial Engineering Journal
ISSN: 0970-2555
Volume : 51, Issue 04, April : 2022

Table 1. Overview of the composition of the various electrodes examined, including the associated post-treatment steps.

	Components	IPA1	IPA 1b	IPA2	IPA3	IPA4	IPA5	Water1	Water 1b	Water2	Water 2b
Solvent	Isopropanol	x	x	x	x	x	x				
	H_2O/ethanol							x	x	x	x
Ink component (binder, pore former, surfactant, ionomer)	PTFE	x	x	x	x	x	x	x	x	x	x
	Methyl cellulose									x	x
	Triton							x		x	
	Sustainion XA-9 (ink)				x	x	x				
Post treatment	Pressed (RT)					x	x				
	Pressed (130 °C)		x	x				x	x	x	x
	Sintered (340 °C)			x				x	x	x	x
	Sustainion XA-9 layer	x	x	x			x	x	x	x	x

CO_2RR [5, 30]. Methyl cellulose is used not only to thicken and stabilize the ink, but also to serve as a pore-forming agent in the catalyst layer [31].

The electrode preparation generally followed a standardized protocol: all ink components except the PTFE powder were dispersed under atmospheric conditions (5 × 1 min) using a high shear mixer/disperser (Ultraturrax) at about 300 W (13 800 rpm). Subsequently, the PTFE powder was added, and the process was repeated.

The thus produced ink was then airbrushed onto the GDL at 80 ˚C. Subsequent post-treatment steps such as pressing and sintering of the electrode were applied upon the spray coating process. For all electrodes, the total loading of the deposited layer, including catalyst and PTFE, was adjusted to 1 mg cm^{-2}. Subsequently, round-shaped electrodes with a diameter of 22 mm were cut out, drop-casted with a Sustainion XA-9 solution and, after drying, immersed in 1 M KOH for at least 24 h.

This protocol was previously shown to lead to an optimal balance between the wetting of the electrode and the generation of C_{2+} products [25]. The ionomer XA-9 as an ion-conducting, hydrophilic ionomer is herein supposed to adjust the wetting properties of the catalyst layer and to suppress the flooding of the electrode by being a physical barrier toward the electrolyte solution. Notably, due to the lack of thermal stability of the SustainionXA-9 (figure S-2), these electrodes were only pressed at RT. Electrodes named with 'b' are repeats provided for comparison with an additional pressing step (electrode IPA1b) or leaving away Triton X (electrodes Water1b and 2b). Their CO_2RR results are shown in the SI section in figure S-8.

Physical properties of the GDEs

Ink formulation

Since spray coating usually requires a dispersion-stable ink where no agglomeration occurs at the relevant timescales of processing, it is essential to elucidate to what extent the inks will keep their initial consistencyduring the entire spraying process.

Thus, investigations on the stability of the inks were performed using an analytical centrifuge (figure S-2) [26]. Notably, only the ink for Water2 electrodes showed elevated stabilityfor over 6 h at 400 rpm (∼21 × g (g-force)). Contrary, all other inks (IPA1/2, IPA3/4/5 and Water1) revealed fast sedimentation within a short time. Comparison with Water1b and Water2b inks produced without Triton shows no noticeable influence of Triton on the ink stability. For an improved understanding of the surface texture of the resulting catalyst layer and the CO_2RR performance of the generated GDEs, the four inks, IPA1/2, IPA3/4/5, Water1, and Water2—all at identical solid concentration—were subsequently investigated by rheology (figure 2).

The flow curves of the inks for the preparation of electrodes IPA1/2, IPA3/4/5, and Water1 are almost identical, showing overall the same degree of shear thinning that can be ascribed to the breakup of CB agglomerates. This finding is in line with reports by Khandavalli *et al*, hypothesizing that weakly charged CB agglomerates form upon collisions induced by Brownian motion [32].

However, it can be anticipated that the microstructure of the catalyst layer is influenced by the properties of the inks, in particular by the degree of agglomeration during the coating step, but also by the interactions between the first layer of deposited particles and the substrate, as well as by particles inside the catalyst layer that come close and determine the structure formation upon drying. From the rheograms it becomes clear that only the inks for Water2 electrodes containing methyl cellulose revealed a Newtonian behavior. These findings suggest that these inks will behave differently during spraying and drying as compared to the other inks.

Industrial Engineering Journal
ISSN: 0970-2555
Volume : 51, Issue 04, April : 2022

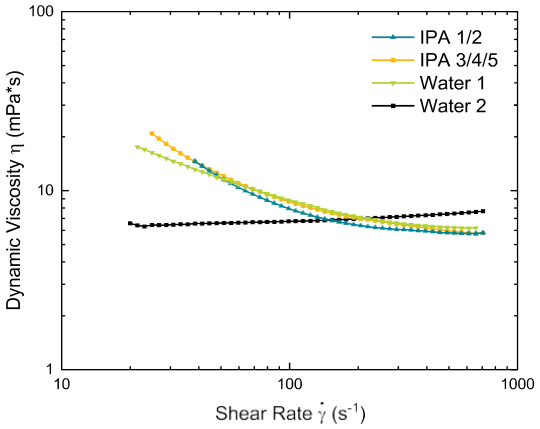

Figure 2. Rheograms of the four inks used for the preparation of catalyst layers.

Table 2. Contact angle measurements of the electrodes with 1 M KOH before and after CO_2RR at 200 mA cm^{-2} over 2 h (triple measurements) as well as crack density, carbonate formation and surface area (by N_2 sorption according to Brunauer–Emmett–Teller (BET). The evaluation in terms of crack density and carbonate formation is to be considered here as a relative assessment between the electrodes tested.

Electrode	Contact angle (before CO_2RR)	Contact angle (after CO_2RR)	Crack density (before CO_2RR)	BET area (before CO_2RR)	Carbonate formation (after CO_2RR)
Water1	153° ± 8°	117° ± 12°	Low	6.4 m^2 g^{-1}	Severe
Water2	159° ± 6°	127° ± 8°	Medium	8.2 m^2 g^{-1}	Limited
IPA1	150° ± 4°	112° ± 22°	High	7.9 m^2 g^{-1}	Severe
IPA2	162° ± 2°	120° ± 11°	Low	8.2 m^2 g^{-1}	Severe
IPA3	130° ± 19°	109° ± 11°	High	7.8 m^2 g^{-1}	Limited
IPA4	149° ± 7°	95° ± 23°	High	8.7 m^2 g^{-1}	Limited
IPA5	149° ± 7°	103° ± 13°	Low	8.7 m^2 g^{-1}	Severe

As-prepared electrodes

To further investigate the influence of the ink compositions, electrodes were prepared following the same procedure as described above. The electrodes and the surface properties of the obtained catalyst layers were then analyzed by scanning electron microscopy (SEM) measurements before and after electrolysis (figure 3). The gained results were related with the ink properties and the post-treatment procedure. Obviously, the ink formulation and the process conditions applied during catalyst layer preparation led to significant morphological differences in the surface structure, including both roughness and cracking.

Comparing the SEM images before CO_2RR, the highest surface roughness is found for electrode Water2, whose ink contained methyl cellulose and Triton. The surface of electrodes IPA2, IPA5, and electrode Water1 is smooth but nevertheless also shows some cracks. While electrode IPA1 reveals an uneven surface with pronounced crack formation (figure 3(a)), electrode IPA2 (figure 3(b)) displays a smooth surface morphology which seems to originate from levelling caused by pressing. Contrary, electrodes prepared without methyl cellulose (electrodes IPA2, IPA4, IPA5, and electrode Water1) showed an ultrathin detachment of the surface layer.

To further investigate the influence of the ink composition and electrode post-treatment on the surface properties of the electrodes, water contact angle measurements were carried out on the assembled electrodes before CO_2RR and without application of a Sustainion XA-9 layer (table 2). The reason for not

Industrial Engineering Journal
ISSN: 0970-2555
Volume : 51, Issue 04, April : 2022

applying the XA-9 layer for the contact angle measurements is that this topping layer would significantly interfere with the measurements due to its hydrophilicity. Hence, the presence of Sustainion XA-9 would prevent the gain of meaningful information about the catalyst layer itself. It can be seen, that for electrodes IPA1 and IPA2 as well as for IPA3 and IPA4, the presence of pressing leads to an increase in the contact angle.

The more even surfaces resulting from pressing, i.e. comparing electrodes IPA1 and IPA2 (figures 3(a) and (b)), lead to higher water contact angles and thus increased hydrophobicity. Interestingly, the contact angles of the electrodes Water1 and Water2 are very close to each other despite the large differences in their surface morphology (figures 3(d) and (e)).

In contrast, water sorption measurements show an altered trend with a higher hydrophobicity for electrode Water1 compared to electrode Water2. Overall, electrodes IPA3, IPA4 and electrode IPA5, with

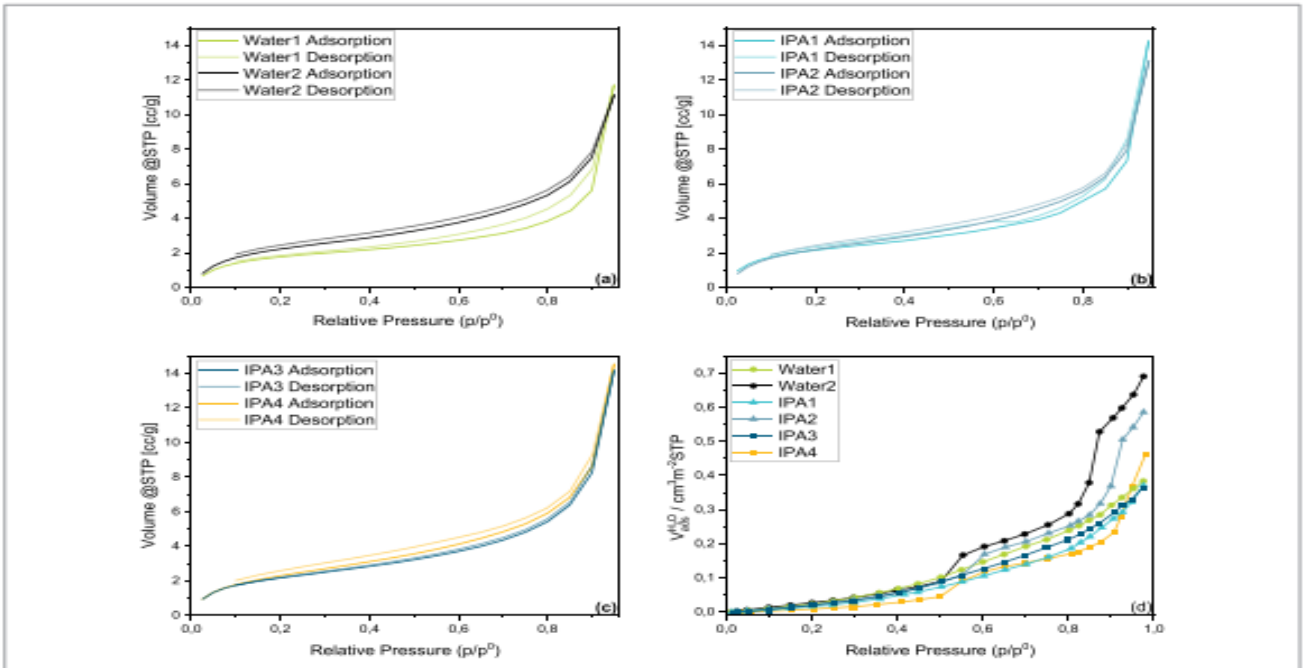

Figure 4. (a)–(c) BET isotherms under N_2 at 77.35 K; (d) BET surface areas—normalized water physisorption isotherms of electrodes Water1, Water2, IPA1, IPA2, IPA3 and IPA4 prepared with different inks and post-treatment procedures

Industrial Engineering Journal
ISSN: 0970-2555
Volume : 51, Issue 04, April : 2022

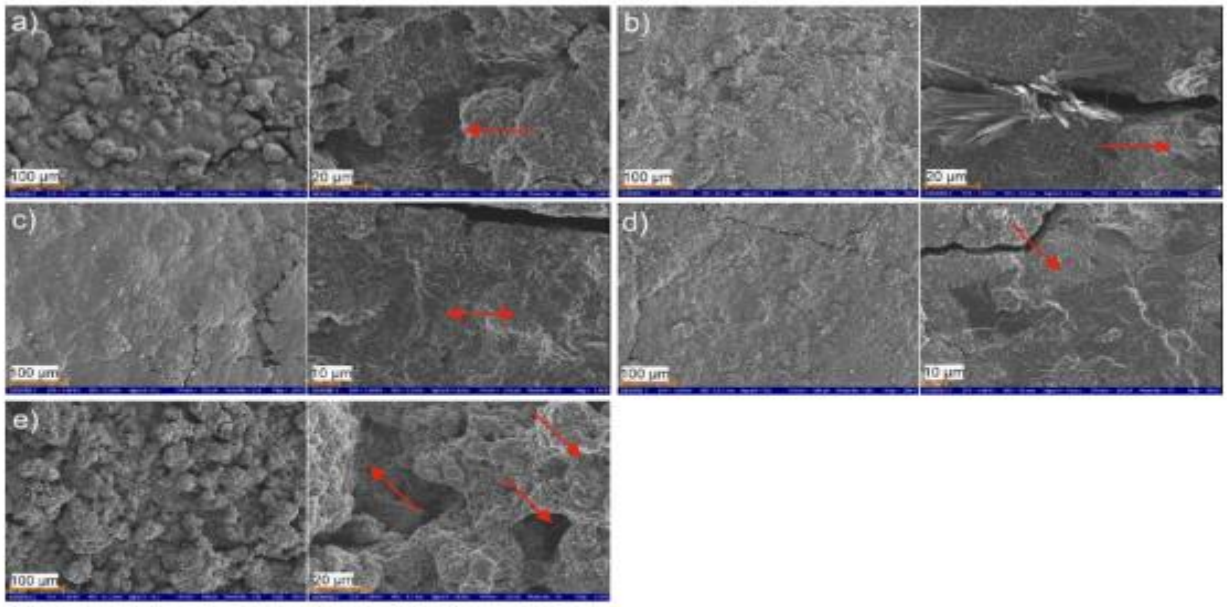

Figure 3. SEM-images of airbrushed electrodes before (200× magnitude, SE2) (left) and after CO_2RR (~1000× magnitude, in lens) (right) (a) isopropanol, no post treatment (electrode IPA1) (b) isopropanol, pressed + sintered (electrode IPA 2) (c) isopropanol + XA-9 in bulk (electrode IPA5) (d) EtOH/H2O + Triton, pressed + sintered (electrode Water1) (e) EtOH/H2O + Triton + Methylcellulose, pressed + sintered (electrode Water2). The red arrows indicate the formation of carbonate crystals.

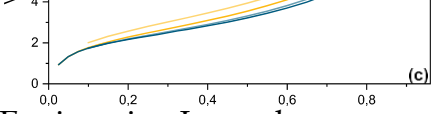

Industrial Engineering Journal
ISSN: 0970-2555
Volume : 51, Issue 04, April : 2022

Sustainion XA-9 directly added to the ink formulation, generally had the lowest contact angles in the tested series. This is in line with our expectations, since Sustainion XA-9 is supposed to increase the wettability ofthe electrode due to its hydrophilic character.
Water sorption measurements (figure 4(d)) also revealed that the bulk hydrophobicity is lower for the pressed electrodes, i.e. electrode IPA2 vs. electrode IPA1 and electrode IPA4 vs. electrode IPA3.

However, only three of the four pressed electrodes, electrode Water2, electrode IPA2 and electrode IPA4show a reduced hydrophobicity with Sustainion XA-9 after CO_2RR. The other electrodes, electrode Water1, electrode IPA1, and electrode IPA3 nearly end up with the same value of around 0.36–0.38 cm^{-3} m^{-2}.

Interestingly, the electrodes Water2, IPA2, and IPA4 show a two-step water sorption process. This behavior can be explained by larger and more hydrophilic pores that fill up with water first, followed by filling the smaller ones. In general, it is notable that the observed trends for contact angle measurements and the bulk hydrophobicity determined via water physisorption are opposite. This shows that surface and bulk properties can differ significantly because of, e.g. surface roughness or different porous structures within the catalyst layer. Thus, the analysis of the surface structure/morphology is not sufficient to allow for a reliable judgement of the electrode composition and setting up structure/activity relationships but must be accompanied by additional methods that give access to the pore network inside the catalyst layer.

In addition, the bulk properties of the GDEs were also determined using nitrogen physisorption measurements (figure 4). All isotherms obtained from the N_2 sorption measurements were evaluated according to the BET method and belong to type II isotherms, i.e. showing a multilayer adsorption. Type II isotherms are typical for non-porous or macroporous substrates with pore diameters above 50 nm. As all isotherms show a rather flat instead of a sharp increase at low pressures, an overlap of the monolayer formation and the multilayer adsorption is anticipated. Especially for electrode Water1 and electrode IPA4, hysteresis loops are visible, which can be associated with capillary condensation [33]. In addition, N_2 sorption measurements (figures 4(a)–(c)) reveal highest surface areas for electrode IPA4 (8.7 m^2 g^{-1}) as compared to electrode IPA2 (8.2 m^2 g^{-1}) and electrode Water2 (8.2 m^2 g^{-1}). Overall, the following BET surfaces were obtained: 6.4 m^2 g^{-1} (electrode Water1), 7.8 m^2 g^{-1}(electrode IPA3), 7.9 m^2 g^{-1} (electrode IPA1), 8.2 m^2 g^{-1} (electrode IPA2), 8.2 m^2 g^{-1} (electrode Water2) and 8.7 m^2 g^{-1} (electrode IPA4).

As it is noted, no clear trend can be deduced from the ink composition and micro structuring of the surfaces linking them with the BET results. This already points toward hidden parameters that must be unraveled in a targeted way in future studies. A major difference to all other electrodes is observed for the surface of electrode Water1, which finally manifests by the results of N_2 sorption, revealing a minimum valuefor the specific surface area of 6.4 m^2 g^{-1}.

Electrodes after electro catalysis

The comparison of the surface morphologies of the electrodes before and after CO_2RR at 200 mA cm^{-2} shows that the surfaces generally exhibit more cracks after electrolysis. Only when methyl cellulose containing inks were used, as in case of electrode Water2 (figure 3(e)), fewer cracks were observed, suggesting a beneficial pore structuring. It is possible that cracks in the catalyst layer support the flooding behavior, since the electrolyte can penetrate more easily into the GDE [34].

Along this line, Kong *et al* compared the CO_2RR of Ag nanoparticles using two different GDLs based on carbon paper. The first GDL using carbon paper from Freudenberg as macroporous layer (MPL) showed a lot of cracks, whereas when carbon paper from Sigracet was used as MPL, a compact and dense surface

was obtained. The performance of the Freudenberg electrode was superior during electrosynthesis and showed an elevated stability due to the direct access of the electrolyte solution to the carbon fiber network. The facilitated access resulted in an enhanced carbonate formation within the fibers instead of blocking the active sites of the catalyst. The authors concluded, that cracks within GDLs can be beneficial for the overall water management [35]. The carbonate precipitation occurs due to the simultaneous presence of CO_2 and OH^- during CO_2RR resulting in the growth of carbonate crystals within the catalytic layer as well as the GDL. In this work, carbonate formation was in particular observed for electrodes IPA1, IPA2, IPA5 and electrode Water1, which showed large areas of the electrode surface (top view) populated with crystals (figures 3(a)–(d) and S-5). In addition, the elemental mapping (figure S-6) showed mainly the presence of potassium and oxygen, but also of copper as rod-shaped crystals. Especially, the needle-shaped copper crystals suggest catalyst leaching during CO_2RR (figure S-6).

Even after CO_2RR, the electrode Water2 (figure 3(e)) showed the most uneven surface and the most cavities. Here, carbonate crystals can also be seen (red arrow) that mostly appear as narrow rods. In contrast and as mentioned before, electrodes produced without methyl cellulose in the ink formulation (figures 3(a)–(d)), showed larger and more cracks and furthermore revealed larger crystals spread out over a large area. SEM-energy dispersive x-ray spectroscopy (EDX) investigations of the electrode surfaces clearly indicate that the crystals consist of potassium carbonate (figure S-5). Notably, electrodes prepared from inks formulated without methyl cellulose showed a relatively uniform crack formation (figure S-5). This could be caused by the damage of the catalytic layer during the electrocatalytic processes, but also due to damage during the subsequent drying of the wetted catalyst layer.

Since EDX measurements showed no zinc after the CO_2RR experiments, a leaching out of the metal during the electrochemical measurements is anticipated. At this point it has to be mentioned that, unfortunately, ICP-OES analysis after CO_2RR is hard to realize for the following reasons:

After CO_2RR additionally to the pure catalyst, PTFE and Sustainion XA-9 are present and therefore need to be separated from the measurement data to assure correct results.

(a) As can be seen from the SEM micrographs, there is an irregular carbonate formation at the catalyst layer, which also falsifies the results.

(b) For an analysis after CO_2RR, the catalyst layer would have to be scraped off the GDL which is hardly doable. The result could be falsified by the separating parts of the microporous layer.

Likewise, ICP-OES analyses of the catholyte solution could not confirm leaching, as no zinc (or copper) was detectable. This points toward a small but continuous dissolution over time into the electrolyte. In addition, although EDX measurements of the electrodes before CO_2RR clearly revealed the presence of Zn (figure S-7), the addition of Sustainion XA-9 before electrocatalysis as well as the formation of potassium-containing crystals on the surface can interfere with the detection of Zn in deeper layers and thus falsify this result. This observation confirms that complicated electrocatalysts can easily dealloy or restructure at higher current densities and thus will eventually provide an altered product spectrum for CO_2RR during aging.

Overall, a decrease in contact angles and thus surface hydrophobicity was observed for all electrodes after

electrolysis. This decrease is not only due to the application of the hydrophilic Sustainion XA-9 top layer. This becomes clear from the electrodes IPA3 and IPA4 as there was no Sustainion XA-9 layer applied before CO_2RR. For those electrodes, the contact angles were significantly smaller and even reached some of the lowest values after electrolysis with a decrease from 130° to 109° and 149° to 95°, respectively. The loss in hydrophobicity during the CO_2RR measurement has repeatedly been described in the literature and can be attributed to several phenomena: (a) degradation of PTFE, (b) erosion of the catalytic layer, (c) formation of carbonates within the GDE, (d) increasing oxygen coverage of carbon surfaces [30, 36, 37]. The largest contact angle is obtained for the electrode Water2 (127°), which was produced with methyl cellulose as a pore forming agent alongside EtOH/H_2O as solvent. Likewise, the SEM (-EDX) images (figures 3 and S-5, S-6) show that hygroscopic potassium salts formed on the electrode surface, which additionally leads to smaller contact angles. Furthermore, the formation of salts and cracks could explain the strong deviations between single contact angle measurements after CO_2RR, since the obtained value heavily depends on the morphology of the electrode surface below the 1 M KOH droplet.

Changes in the surface morphology due to salt and crack formation were observed and were the smallest for electrode Water2. These small deviations in the hydrophobicity are also mirrored in the tested electrode itself and increase the overall stability of the electrode during electrolysis.

In general, effective CO_2RR gas-water pathways within the catalyst layer, created by hydrophobic additives like PTFE, are necessary to ensure CO_2 and product transport [30]. Furthermore, the roughness and morphology of the surface of the catalyst layer (top view) strongly influence the hydrophobic behavior of the surroundings. Hence, with enhanced roughness, surfaces showed an increased hydrophobicity.

Electrochemical characterization

Investigations on the electrochemical CO_2RR were performed by chronopotentiometric measurements, where electrodes were placed into an electrochemical flow cell (figure S-4). In brief, the catalyst layer faces the 1 M KOH electrolyte solution, while the GDL faces the gas compartment where CO_2 is supplied. All electrochemical measurements were performed over 2 h at 200 mA cm^{-2} at RT.

The electrolyte solution was circulated through the cathode and anode chamber, respectively, to prevent a partial temperature increase, to transport formed products away from the electrodes, and to provide fresh electrolyte to the electrode surface. As the objective is to increase the FE_{C2+}, especially ethanol and ethylene, the scope of the following discussion is focused mainly on these products.

To determine the stability of the utilized electrodes and their selectivity for C_{2+} products, gas samples were collected every 20 min over the course of 2 h by a coupled online gas chromatography-mass spectrometry (GC-MS) system with liquid analysis being performed after the electrolysis. In addition to the different surface morphologies and hydrophilicities, the CO_2 reduction itself is strongly influenced by the chosen process chain, i.e. the composition of the different inks used for the preparation of the different catalyst layers and the subsequent post-treatments of the generated electrodes. The total FEs resulting from the 2 h electrolysis for the different electrodes are shown in figure 5(a).

By changing the ink composition as well as the post treatment of the electrodes, the FE for the CO_2RR can be heavily altered. Specifically, for the formation of ethanol, an increase from 0% (electrode IPA3 and

Industrial Engineering Journal
ISSN: 0970-2555
Volume : 51, Issue 04, April : 2022

electrode IPA4) up to 11.2% for electrode Water2 can be achieved and is in line with the larger contact angles (table 2) and thus higher surface hydrophobicity.

In addition, SEM images showed significantly fewer cracks for electrode Water2 than for the others andalso the formation of fewer crystals covering larger areas (figures 3 and S-5). For electrode Water2, C_{2+}

Industrial Engineering Journal
ISSN: 0970-2555
Volume : 51, Issue 04, April : 2022

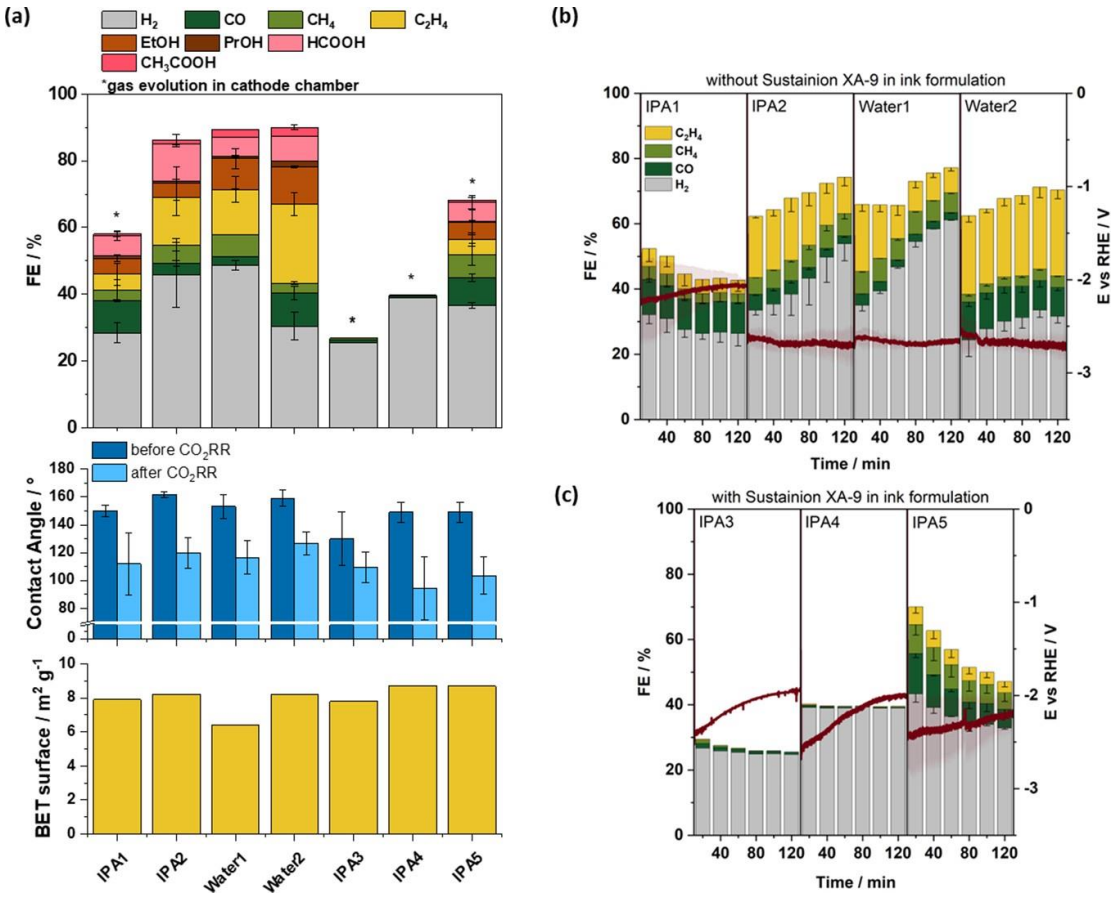

Figure 5. Comparison of total FEs for GDEs made from different ink formulations (isopropanol or EtOH/H_2O based electrodes IPA1, IPA2, Water1, Water2, IPA3, IPA4 and IPA5) and post treatments. GDEs were measured at 200 mA cm^{-2} for 2 h in 1 M KOH, the gas products are averaged over 2 h measurement and FEs are shown in relation to the electrodes contact angle and BET surface (multi-point BET) in terms of (a); (for BET: a maximum weighing error of 1 mg is anticipated as error); product distribution when using the generated electrodes during 2 h electrolysis with corresponding chronopotentiometry curves (potential vs. RHE, dark red line, linked to right y-axis; data without iR correction) for inks without (b) and with Sustainion XA-9 (c).

products with an average FE of 39.5% were observed. In general, figure 5(a) shows, with regard to electrodes IPA1 and IPA2, that pressing and sintering of the electrode indeed has a significant effect on the surface morphology (figures 3(a) and (b)) as well as on the FEs of CO_2RR products. For electrode IPA1, a noticeable gas formation at the GDE toward the cathode electrolyte compartment was visible during electrolysis. Since KOH is used as the electrolyte, the product gas stream cannot be passed over the catholyte again to also analyze the product gases there. This would directly lead to the formation of carbonates. Therefore, the catholyte gas space was not analyzed in this setup. The total FE reached was under 53%, but nevertheless, theFE for ethanol was 4.8% for electrode IPA1. The electrode IPA2 was sprayed using the same ink as in the caseof electrode IPA1, but additionally, it has been post-pressed and sintered. These post-treatment steps, which also levelled the surface of the therewith generated electrodes (figures 3(a) and (b)), seem to have stabilized the electrodes' performance, giving overall FEs of almost 90%. In addition, a shift in the product spectrum can be observed for electrode IPA2 as the formation of CO is lower than in case of electrode IPA1 and an increase in methane and ethylene formation occurred. Notably, the FE_{CO} increased from 3.2% (electrode IPA1) to 14% (electrode IPA2), while the FE of CH_4 increased

from 3.1% to 5.6% and the FE for ethylene even from 4.7% to 14.2%. Combining these observations with the earlier findings on contact angles (table 2), it becomes clear that the increased formation of CO_2RR products correlates with a higher hydrophobicity of the surface for the electrode. We suggest to take this as a first design rule for CO_2RR electrode manufacturing. Control experiments with the electrode IPA1b showed that pressing has a stabilizing effect on the electrode performance and higher FEs are achieved for products like ethylene in comparison to electrode IPA1 (5.2% vs. 4.7%) as well as methane (7.6% vs. 3.1%) and ethanol (5.7% vs. 4.8%). However, the FEs for the CO_2RR products increase further with the additional sintering of electrode IPA2. Probably, as a result of the sintering process at 340 °C, oxidation of the copper occurred. It is known from the literature that the reduction of copper oxides under the CO_2RR conditions and the resulting defects and grain boundaries may increase the surface activity [13].

The post-treatment of electrode IPA2 led to higher contact angles of 162° (before) and 120° (after electrolysis) compared to electrode IPA1 with 150° and 112°, respectively. However, there was a slight decrease in the FE for ethanol, which dropped from 4.8% to 4.2%. Nevertheless, among all the electrodes presented here, electrode IPA2 showed the highest formation of formic acid of 11.2%. Comparison of the Sustainion containing electrodes IPA3 and IPA4 exhibited strong gas evolution toward the cathode compartment and in addition, on-line GC-MS analysis showed hydrogen being the main product.
Post-pressing seems to have a minimal effect on the gas evolution toward the cathode compartment. Total FEs were obtained for electrode IPA4 of about 40% in contrast to about 35% for electrode IPA3, with the total FE toward CO_2RR products being <1.6% in either case. Although the presence of post-treatment again resulted in higher hydrophobicity for electrode IPA2 in contrast to IPA1 (table 2), no increased formation of CO_2RR products was observed. Drop casting with Sustainion XA-9 improved this behavior considerably.

With electrode IPA5 ethanol FEs of 5.1% were achieved while the rest of the CO_2RR spectrum comprised ethylene (FE 4.5%), CO (FE 8.3%) and CH_4 (FE 7.0%).
As noted, the best CO_2RR results were obtained with electrodes made from EtOH/H_2O-based inks, i.e. electrode Water1 and electrode Water2. In addition, the effect of Triton (for electrode Water1) and Triton/methyl cellulose (for electrode Water2) was investigated. Both, electrodes Water1 and Water2 showed the best CO_2RR results among all tested electrodes, with FEs of 9.3% and 11.2% for ethanol and 13.5% and 23.7% for ethylene, respectively. Interestingly, FEs of 2.2% and 2.7% for acetic acid and 0.7% and 1.8% for propanol were achieved for electrodes Water1 and Water2, respectively. Particularly striking is the relatively high value for the formation of methane at electrode Water1, with 6.7%. Likewise, electrode Water2 showed a very high yield for CO_2RR products in general, which has been accompanied by low FEs for the HER of solely 30%. Control electrodes prepared without Triton (electrodes Water1b and Water2b, figure S-8) in the ink showed a lower formation of C_{2+} products than the electrodes Water1 and Water2. FE_{EtOH} of 9% and $FE_{ethylene}$ of 7% were achieved for electrode Water1b, 10% and 19% for electrode Water2b, respectively. Along this line, it has been shown previously for pure Cu-GDEs, that varying the ink composition, as by changing the solvent, has an effect on the microstructuring of the GDE. The reason is that the used solvent affects how binders and catalyst particles interact with each other [34].

In figures 5(b) and (c) the composition of gas products over the course of the 2 h experiment is shown, with the gas stream examined every 20 min by online GC-MS. In addition, the averaged course of the chronopotentiometry curves from the CO_2RR for the different electrodes is displayed. For the chronopotentiometry curves, a change in voltage towards more positive values can be associated with flooding of the GDE [38]. During the flooding, the diffusion paths of the CO_2 are blocked by carbonate formation in the electrode. When the electrolyte solution has penetrated the entire electrode, the transport

of CO_2 toward the catalyst surface is limited by its solubility in the electrolyte. Due to the wetting of more electrode surface with the electrolyte solution, a higher active area is obtained, resulting in a more positive potential. In these cases, consequently, a significant increase in H_2 formation is also observed, while the CO_2RR decreases. A very significant increase in voltage can be observed for the electrodes IPA1, IPA3, IPA4, and electrode IPA5 (figures 5(b) and (c)). The increase in voltage over time suggests that in addition to the mentioned observations from literature, the presence of cracks may not only increase the mass transport but also promote flooding of the electrode. Furthermore, a visibly stronger gas evolution toward the cathode chamber was observed, which probably constitutes of mainly hydrogen formation. Especially for electrode IPA5, but also for the other two electrodes IPA3 and IPA4 with Sustainion XA-9 in the bulk, a decrease of the CO_2RR product formation over time is noticeable. The lower CO_2RR for electrodes IPA1-5 and Water1 compared to electrode Water2 is accompanied by the increased formation of carbonates on top and inside the catalyst layer, as discussed previously (figures 3 and S-5).

The comparison of electrodes IPA3, IPA4, and IPA5 also shows the influence of the coating of the electrode with a Sustainion XA-9 layer. In the case of electrode IPA5, the additional layer results in a flatter chronopotentiometry curve which indicates a significantly more inhibited flooding behavior. In addition, similar to our previous results on Cu-GDEs, the Sustainion XA-9 layer optimizes the local environment and wetting of the electrode, significantly favoring the CO_2RR [25]. With regard to electrode IPA1, it is also apparent from both the course of the chronopotentiometry curve and the gas product distribution, that post-treatment of the electrode by means of pressing and sintering (electrode IPA2 vs. electrode IPA1) can significantly improve the overall CO_2RR performance. The resulting potential curve for electrode IPA2 shows a more stable behavior and the potential remains at an approximately constant level in the range of
−2.6 to −2.7 V (not iR corrected) during the 2 h period. As previously discussed, this behavior indicates a decreased tendency of the electrode towards flooding. This is simultaneously associated with an elevated production of CO_2RR products, especially C_{2+}, over time. Nevertheless, for electrode IPA2 a decrease of the CO_2RR product formation is noticeable, such as ethylene with a FE of 18.8% after 20 min to 11.2% after 2 h with a simultaneous increase of H_2 formation from 33.5% to 53.8%. Thus, a progressive flooding occurs within the duration of the experiment of 2 h.

As the thickness of the catalyst layer is known to affect the local concentration of CO_2 and therefore the CO_2RR product distribution, the thickness of the catalyst layer of electrode Water2 was systematically varied (figure S-9). This was realized by adding additional layers of catalyst and thus also achieving a varying catalyst loading of 0.5, 1, and 1.3 mg cm^{-2}. At 0.5 mg cm^{-2} (the thinnest electrode), the lowest FEs for CO_2RR were observed. Moreover, the passage of CO_2 through the GDE into the catholyte occurred. The overall yield of C_{2+} products was approximately 13%. At 1.3 mg cm^{-2} (the thickest electrode), a drop in CO_2RR products in favor of HER was observable. The overall FE of C_{2+} products decreased from about 40%–33%.
Regarding the long-term stability of the EtOH/H_2O electrodes (electrodes Water1 and Water2), a generally higher H_2 production as electrolysis progresses is observed. In contrast, electrode Water2 showed a stable potential curve (at about −2.7 V) without any voltage increase. In addition, the hydrogen formation remained clearly more constant over time and always ranged between 24.3% and 33.5%. The formation of the CO_2RR products showed a slight increase in CH_4 formation from 2.4% to 3.5%, while at the same time the FE_{CO} decreases slightly from 11.7% to 9.4%. The FE for ethylene was in the range of 23%–26.4%. The electrode Water2 showed both the best FEs for CO_2RR products and, according to the SEM images, the uneven surface with the most pores (figure 3(e)). In addition, the contact angles after electrolysis of 127° showed that in comparison to other electrodes, the electrode Water2 experiences a decreased loss in

Industrial Engineering Journal
ISSN: 0970-2555
Volume : 51, Issue 04, April : 2022

hydrophobicity over the measurement period of 2 h compared to other electrodes (see table 2). In addition, the SEM images after electrolysis showed significantly fewer crystals and cracks than in case of all other electrodes of this study.

Implications for electrode assemblies

In terms of electrochemical performance, the comparison of the isopropanol and water/ethanol-based inks shows that for the latter higher FEs were obtained for CO_2RR products. These higher FEs occur although no notable trends with respect to BET surface areas or hydrophobicity emerge.

Furthermore, the observed morphology differences suggest that the absence of methyl cellulose as pore forming agent leads to an overall smoother surface as is visible when comparing electrode Water1 (d) and electrode Water2 (e) in figure 3. The use of methyl cellulose as pore-forming agent stabilized the ink decisively and at the same time resulted in an increased BET surface area and a much rougher surface.

During CO_2RR, the usage of the electrode made from an ink containing methyl cellulose also exhibited the lowest flooding behavior and resulted in the highest yield of C_{2+} products, particularly EtOH and ethylene.

Addition of Sustainion XA-9 as well as Triton X-100 to the ink had no significant influence on the surface texture (top view). The addition of Sustainion XA-9 generally resulted in a more hydrophilic surface (contact angle measurements), but led to a more hydrophobic bulk material. It is possible that the added ionomer herein alters the pore structure inside the catalyst layer (CL), resulting in the altered hydrophobicity. The addition of Sustainion XA-9 also led to faster flooding of the electrode and reduced formation of CO_2RR products, particularly $C_{2+,}$ probably due to the lower hydrophobicity of the electrode. The usage of Triton had no impact on ink stability, however, electrodes Water1b and Water2b (without Triton) showed less C_{2+} product formation and higher HER in comparison to electrodes containing Triton. Herein, the addition of Triton might have influenced the microstructuring of the catalyst layer and therewith affected the product distribution during electrolysis. Drop casting of the electrodes with Sustainion XA-9 prior to CO_2RR has a crucial influence. As described by Junge Puring *et al*, this provides an additional barrier that reduces electrode flooding and increases the CO_2RR production [25].

Concerning post-treatment of the electrodes, it is visible that the absence of a sintering step results in higher BET surfaces as is notable for electrode IPA5. Herein, the temperature is not high enough to allow for the decomposition of Sustainion XA-9 which was subsequently supported by TG-DTA measurements (thermogravimetric analysis—differential thermal analysis, figure S-3). Still sintering seems to have a less significant effect on the physical properties of the electrodes in the absence of methyl cellulose. The comparison of electrodes IPA1, IPA1b and IPA2 shows a stabilization due to the post-pressing, but largest differences are observed due to the sintering process, which results in a significant increase of CO_2RR products, especially ethylene. For post-pressed electrodes, a potential stabilization was observed and less gas was released into the cathode compartment during electrolysis with higher FEs for CO_2RR products. At both elevated and RT pressing methods, a significant levelling was observed for the surface of the catalyst layer. This becomes clear from the flatter surface morphology and larger BET surface area that were obtained for the non-sintered electrode pressed only at RT.

2. Conclusion

In this work, CO_2RR was performed using Cu-ZnO-CB GDEs manufactured from different inks and utilizing pressing and sintering as post-treatment methods. Herein we show that solvents used to prepare the catalyst inks will eventually lead to an alteration of the electrode structure and morphology equally as the use of additional additives like pore forming agents or ionomers. Likewise, post-treatment of the freshly

prepared electrodes, namely pressing and sintering in comparison with unprocessed electrodes was evaluated.

We show that these post-treatment strategies are equally important than the ink formulation and the catalyst to achieve a certain performance. In summary, the best results were obtained when catalyst layers were spray coated with inks based upon a water-ethanol based solvent mixture and in the presence of additives that were able to establish proper pore structures, i.e. pore-forming agents. Especially, electrodes post-treated by hot pressing methods showed a higher surface hydrophobicity after CO_2RR and also displayed higher CO_2RR activity along with higher C_{2+} product formation compared to GDEs without post treatment. Thus, under the herein presented experimental conditions, a stable CO_2RR performance with FEs for ethanol and ethylene of up to 11.2% and 23.7%, respectively, at 200 mA cm^{-2} was obtained. Yet, lowering the flooding behavior and therefore HER is still a critical issue that needs to be resolved in the future.

In summary, we herein show that the ink composition and post-treatment of GDEs have a significant impact on the stability and electrochemical performance of GDEs. Deciphering these manifold influencing factors in a multidimensional parameter space requires coherent workflows and detailed, highly systematic studies. This will be established and discussed in the near future.

Industrial Engineering Journal
ISSN: 0970-2555
Volume : 51, Issue 04, April : 2022

3. Experimental section

Materials

Copper(II)acetate hydrate (98%, Alfa Aesar), zinc(II)acetate dihydrate (⩾99%, VWR), ENSACO 250 G CB (Imery's Graphite & Carbon), DyneonTM PTFE Powder TF 1750 (3 M) and KOH (p.a., Merck) were used as received from the commercial vendors. Furthermore, Sustainion XA-9 Alkaline Ionomer 5% in ethanol (Dioxide Materials) and Carbon Cloth GDLs with MPL (W1S1011, FuelCellStore) were used for electrode preparation.

Catalyst synthesis

The catalyst synthesis was carried out according to a procedure described by the following literature reports [25]. To receive 10% metal loading related to CB, Cu(II)- and Zn(II)-acetate (mass ratio Cu: Zn 85:15) were dissolved in 500 ml deionized water. Subsequently, 9 g CB was added, and the suspension was sonicated for 3 h. Then, the water was removed via rotary evaporation and the resulting precursor was dried overnight at 105 ˚C and mortared. The precursor powder was placed between glass wool within a glass reactor in a tubular furnace, flushed with N_2 for 10 min at RT and afterwards reduced in H_2 atmosphere at 250 ˚C for 5 h. Cooling to RT was then carried out again under N_2 flushing.

Electrode preparation

The impregnated CB catalyst was processed into different inks. In a representative example, 0.5 g of the catalyst was used, and 30 ml isopropanol was weighed in centrifuge tubes (50 ml) and mixed via a shear mixer/disperser (IKA T18 digital Ultra TURRAX) (five times for 1 min at 13.800 rpm, 1 min pause). Subsequently, 0.055 g PTFE powder was added and mixing (five times for 1 min at 13.800 rpm) was repeated.

The process for making each of the inks followed the principle that first, everything except PTFE was weighed in, mixed, and afterwards PTFE was added. Then, the mixing process was repeated using the Ultraturrax. For the electrodes containing Sustainion XA-9 in bulk, 133 μl were added to the ink (besides isopropanol, catalyst, and PTFE). The EtOH/H_2O-based inks consisted of 0.5 g catalyst, 5.4 ml MilliQ water, 15 ml ethanol, 0.15 g Triton X 100 and 10 g 1 wt.% aqueous methyl cellulose solution as well as 0.55 g PTFE powder. In case of EtOH/H_2O-based inks without methyl cellulose solution, 15 ml MilliQ were used. All inks were airbrushed using an Iwata-Eclipse airbrush pistol and a nitrogen pressure of 1 bar onto a 10 10 cm^2 carbon cloth, which was heated to 80 ˚C. The electrodes were repeatedly weighed to ensure that a loading of 1 mg cm^{-2} was achieved. The dried electrode was then either used as prepared or placed between baking paper and pressed at 40 bar (0.45 kN cm^{-2}), 130 ˚C for 90 s using a Polystat 300S laboratory-scale press. In the case of sintering, the electrode was placed within a muffle furnace and sintered for 15 min at 340 ˚C. The sintering temperature of 340 ˚C was chosen as it is just below the melting point of PTFE. In such a way, the PTFE only 'softens' and induces improved bonding. Higher temperatures could lead to a full closure of the pores by liquid PTFE or decomposition of the binder. The lower pressing temperature as compared to the PTFE melting point was likewise selected for the pressing process, because the press cannot technically be operated at 340 ˚C and no decomposition of components such as methyl cellulose should take place during pressing.

From the different electrodes, 22 mm circular electrodes were cut out and each of those was drop coated with 133 μl Sustainion XA-9 and dried overnight under atmospheric conditions. Before electrocatalysis

Industrial Engineering Journal
ISSN: 0970-2555
Volume : 51, Issue 04, April : 2022

experiments, the electrodes were put into 1 M KOH for activation for 24 h by converting the Cl^- form of Sustainion XA-9 into the OH^- form.

Industrial Engineering Journal
ISSN: 0970-2555
Volume : 51, Issue 04, April : 2022

Electrochemical characterization and product analysis

The electrochemical characterization was performed using an inhouse-built three compartment cell with a cathode and anode chamber being separated by a Fumasep F-10120-PK membrane. The prepared GDEs were used as cathodes with catalyst facing the electrolyte solution. A nickel wire was utilized as counter electrode and a reversible hydrogen electrode (HydroFlex®) was used as a reference electrode for electroless potential determination. For all experiments, 1 M KOH was used as electrolyte. Electrolysis was then performed by chronopotentiometry. The geometric active area was 2.011 cm^2 and 200 mA cm^{-2} were applied. The GDE was then fed with CO_2 and Ar as internal standard on the gas side. The CO_2 flow rate was
22.5 ml min^{-1} (for Ar 2.5 ml min^{-1}), and the backpressure was set to be 25 mbar during the electrolysis experiment. Between the cell and the GC, the gas stream was purged through a water-filled, ice-cooled trap to accumulate condensable products and to detect product crossover through the GDE. All measurements were carried out using a Gamry Interface 1010 potentiostat and a GC-MS QP2020 (Shimadzu; carrier gas helium; column: Carboxen 1010 PLOT from Supelco).

Acid products were analyzed using an Agilent Technologies HPLC 1200 with diode array detector (DAD detector 210 nm R_{eff} 360 nm) and a Phenomenex Rezex ROA-Organic Acid H+ (8%) 250 × 4.6 nm column.The injection volume was 20 μl, the column temperature was 60 ˚C, and 5 mM H_2SO_4 was used as eluent with a flow rate of 0.2 ml min^{-1}. The electrolyte samples were diluted with 5 mM H_2SO_4.
An Agilent 7890B gas chromatograph with MSD 5977B and Agilent 7697A headspace sampler was used for alcohol analysis and 2.5 ml of the sample was placed in a headspace vial, mixed with an internal standard solution. A DB 624 UI 30 m × 0.32 mm × 1.8 μm was used as the column.

Physical characterization

Rheological investigations were carried out using a Modular Compact Rheometer-102 (Anton Paar). A cone/plate attachment has been used.
SEM-EDX measurements were carried out using a ZEISS Gemini2 Merlin. SEM images were recorded at 5 kV, for SEM-EDX 20 kV were used. The electrodes were coated with carbon before.
X-ray diffraction was performed using a PANalytical X-Pert MPD with Cu-Kα radiation at 45 kV and 40 mA without using a monochromator. A step size of 0.79 s per step was chosen.

For the determination of metal loading by ICP-OES, the catalyst was first dried at 105 ˚C in a drying oven, then 100 mg of the sample was digested with 10 ml of HNO_3 Suprapur in a microwave at 230 ˚C for 30 min. ICP-OES measurements were performed using an 'Arcos' device with radial plasma. For every measurement as an internal standard, 20 mg l^{-1} yttrium was added to each sample and each calibration solution serving as a blank.

The evaluations were carried out using the Cu emission lines λ = 324.754 nm and λ = 327.396 nm and the Zn emission lines λ = 213.856 nm and λ = 206.200 nm. For calibration, 11 different Cu and Zn containing standards were used, with concentrations ranging between 0 and 40 mg l^{-1}.

Data availability statement

The data generated and/or analyzed during the current study are not publicly available for legal/ethical

reasons but are available from the corresponding author on reasonable request.

References

[1] Daiyan R, Saputera W H, Masood H, Leverett J, Lu X and Amal R 2020 A disquisition on the active sites of heterogeneous catalysts for electrochemical reduction of CO_2 to value-added chemicals and fuel *Adv. Energy Mater.* **10** 1902106

[2] Masel R I, Liu Z, Yang H, Kaczur J J, Carrillo D, Ren S, Salvatore D and Berlinguette C P 2021 An industrial perspective on catalysts for low-temperature CO_2 electrolysis *Nat. Nanotechnol.* **16** 118–28

[3] Salvatore D A *et al* 2021 Designing anion exchange membranes for CO_2 electrolysers *Nat. Energy* **6** 339–48

[4] Burdyny T and Smith W A 2019 CO_2 reduction on gas-diffusion electrodes and why catalytic performance must be assessed at commercially-relevant conditions *Energy Environ. Sci.* **12** 1442–53

[5] Gawel A, Jaster T, Siegmund D, Holzmann J, Lohmann H, Klemm E and Apfel U-P 2022 Electrochemical CO_2 reduction—the macroscopic world of electrode design, reactor concepts & economic aspects *iScience* **25** 104011

[6] Martić N *et al* 2020 $Ag_2Cu_2O_3$—a catalyst template material for selective electroreduction of CO to C_{2+} products *Energy Environ. Sci.* **13** 2993–3006

[7] Wang P, Yang H, Xu Y, Huang X, Wang J, Zhong M, Cheng T and Shao Q 2021 Synergized Cu/Pb core/shell electrocatalyst for high-efficiency CO_2 reduction to C_{2+} liquids *ACS Nano* **15** 1039–47

[8] Ma W, Xie S, Liu T, Fan Q, Ye J, Sun F, Jiang Z, Zhang Q, Cheng J and Wang Y 2020 Electrocatalytic reduction of CO_2 to ethylene and ethanol through hydrogen-assisted C–C coupling over fluorine-modified copper *Nat. Catal.* **3** 478–87

[9] García de Arquer F P *et al* 2020 CO_2 electrolysis to multicarbon products at activities greater than 1 A cm^{-2} *Science* **367** 661–6

[10] Li Y C *et al* 2019 Binding site diversity promotes CO_2 electroreduction to ethanol *J. Am. Chem. Soc.* **141** 8584–91

[11] Zhang T, Li Z, Zhang J and Wu J 2020 Enhance CO_2-to-C_{2+} products yield through spatial management of CO transport in Cu/ZnO tandem electrodes *J. Catal.* **387** 163–9

[12] Da Silva A H, Raaijman S J, Santana C S, Assaf J M, Gomes J F and Koper M T 2021 Electrocatalytic CO_2 reduction to C_{2+} products on Cu and CuxZny electrodes: effects of chemical composition and surface morphology *J. Electroanal. Chem.* **880** 114750

[13] Jaster T, Gawel A, Siegmund D, Holzmann J, Lohmann H, Klemm E and Apfel U-P 2022 Electrochemical CO_2 reduction toward multicarbon alcohols—the microscopic world of catalysts & process conditions *iScience* **25** 104010

[14] Yu J, Wang J, Ma Y, Zhou J, Wang Y, Lu P, Yin J, Ye R, Zhu Z and Fan Z 2021 Recent progresses in electrochemical carbon dioxide reduction on copper-based catalysts toward multicarbon products *Adv. Funct. Mater.* **31** 2102151

[15] Hoang T T H, Verma S, Ma S, Fister T T, Timoshenko J, Frenkel A I, Kenis P J A and Gewirth A A 2018 Nanoporous copper-silver alloys by additive-controlled electrodeposition for the selective electroreduction of CO_2 to ethylene and ethanol *J. Am. Chem. Soc.* **140** 5791–7

[16] Song Y, Junqueira J R C, Sikdar N, Öhl D, Dieckhöfer S, Quast T, Seisel S, Masa J, Andronescu C and Schuhmann W 2021 B-Cu-Zn gas diffusion electrodes for CO_2 electroreduction to C_{2+} products at high current densities *Angew. Chem.* **60** 9135–41

[17] Xie L, Liang J, Priest C, Wang T, Ding D, Wu G and Li Q 2021 Engineering the atomic arrangement of bimetallic catalysts for electrochemical CO_2 reduction *Chem. Commun.* **57** 1839–54

[18] Wang S, Kou T, Baker S E, Duoss E B and Li Y 2020 Recent progress in electrochemical reduction of CO_2 by oxide-derived copper catalysts *Mater. Today Nano* **12** 100096

[19] Dinh C-T *et al* 2018 CO_2 electroreduction to ethylene via hydroxide-mediated copper catalysis at an abrupt interface *Science* **360** 783–7

[20] Gabardo C M, O'Brien C P, Edwards J P, McCallum C, Xu Y, Dinh C-T, Li J, Sargent E H and Sinton D 2019 Continuous carbon dioxide electroreduction to concentrated multi-carbon products using a membrane electrode assembly *Joule* **3** 2777–91

[21] Löwe A, Rieg C, Hierlemann T, Salas N, Kopljar D, Wagner N and Klemm E 2019 Influence of temperature on the performance of gas diffusion electrodes in the CO2 reduction reaction *ChemElectroChem* **6** 4497–506

[22] Shaughnessy C I, Sconyers D J, Kerr T A, Lee H-J, Subramaniam B, Leonard K C and Blakemore J D 2019 Intensified electrocatalytic CO_2 conversion in pressure-tunable CO_2-expanded electrolytes *ChemSusChem* **12** 3761–8
[23] Edwards J P, Xu Y, Gabardo C M, Dinh C-T, Li J, Qi Z, Ozden A, Sargent E H and Sinton D 2020 Efficient electrocatalytic conversion of carbon dioxide in a low-resistance pressurized alkaline electrolyzer *Appl. Energy* **261** 114305
[24] Mowbray B A W, Dvorak D J, Taherimakhsousi N and Berlinguette C P 2021 How catalyst dispersion